Topological transitions in magnetized plasma and optical isolators based on leaky waveguide plasmon mode

Ning Han,[1] Jianlong Liu,[2,*] Yang Gao,[3] Keya Zhou,[1] and Shutian Liu[1,†]

[1]*School of Physics, Harbin Institute of Technology, Harbin 150001, China*

[2]*Key Laboratory of In-Fiber Integrated Optics of Ministry of Education, College of Physics and Optoelectronic Engineering, Harbin Engineering University, Harbin 150001, China*

[3]*College of Electronic Engineering, Heilongjiang University, Harbin 150080, China*

(Received 21 February 2022; revised 3 August 2022; accepted 11 October 2022; published 21 October 2022)

Topological transitions open a fundamentally new route of research with interesting optical phenomena in photonic metamaterials. In this work, we comprehensively investigate the topology of equifrequency surfaces in magnetized plasma. The full topological phase diagrams are shown and the critical points in the topological transitions are given. The equifrequency surfaces evolve from the closed-form ellipsoid to the open forms type-I or type-II hyperboloid in the topological transitions. Remarkably, a type of nonreciprocal optical isolator is demonstrated utilizing the transformation from topological surface states to leaky modes in magnetized plasma. Our work may provide additional insights into topological wave physics and the novel optical isolator has potential applications in light modulation.

DOI: 10.1103/PhysRevB.106.165306

I. INTRODUCTION

Topology is highly robust in conserved quantities. It does not change when physical objects are continuously deformed [1–7]. Topological ideas in photonics originated from solid-state materials, and then a new phase called photonic topological insulators was found [8–13]. In recent years, the realization of photonic topological insulators in chiral metamaterials [14–16], photonic crystals [17–21], and magnetized plasma [22,23] has become the focus of attention. Particularly, the remarkable feature of photonic topological insulators is the existence of the topological surface states [14]. The surface waves can transmit perfectly on the boundary between two media with different topological properties [15]. Moreover, Weyl semimetals possess gapless-type band structures in three-dimensional (3D) systems [2,24,25]. An important characteristic of the Weyl semimetals is the existence of the Fermi arc connecting Weyl points with opposite chirality in momentum space [25].

The propagation of light in the media can be determined by the equifrequency surface, which is similar to the Fermi surface of electrons in crystals [26]. Different from the regular spherical and ellipsoidal shapes known in natural media, singular equifrequency surfaces can be designed in photonic metamaterials [27–30]. A large number of unconventional optical properties can be produced by engineering the exotic equifrequency surface in metamaterials, such as spontaneous emission, subdiffraction imaging, and nanoscale resonator [31]. In the phase space of constant frequency electromagnetic waves, different types of equifrequency surfaces represent dissimilar topological properties [32,33]. According to the definition, every equifrequency surface belongs to a class of quadric surfaces, and the topology of the equifrequency surface governs wave dynamics inside media [32]. By altering the topology of equifrequency surfaces in photonic metamaterials, a new approach to controlling light-matter interactions could be provided [27]. Generally, nondegenerated forms of equifrequency surface in photonics can be classified as ellipsoid and hyperboloid, and different types of equifrequency surfaces cannot be smoothly transformed into each other (topological transition). In Ref. [33], topological transition in the biaxial gyroelectromagnetic metamaterial depends on periodic structure, and the thicknesses of the layers satisfy the long-wavelength limit. Moreover, photonic topological phases based on the equifrequency surfaces in metamaterials have been proposed and demonstrated [14,34–38].

In modern optical technologies, nonreciprocal light transmission plays a key role [39]. Optical isolators are devices that allow light to pass in one direction while blocking transmission in the other direction [40–53]. It is usually required to break the Lorentz reciprocity [43]. Recently, optical isolators based on the magneto-optical effect in photonic crystals have been investigated [40,51,52], which usually use strict periodic structures. On the other hand, optical isolators can also be achieved in systems that do not rely on strictly periodic structures, such as double-layer graphene on magneto-optic substrates [53]. In particular, the mechanism of optical isolation (resonant coupling) between the one-way waveguides and cavity is through a single-mode resonator (cavity) in Ref. [40]. Compared with photonic crystals, magnetized plasma is a simple natural electromagnetic continuum medium [24], and the magnetized plasma has nonradiative chiral surface modes on its surface that do not depend on metal claddings [38]. Generally, metal cladding such as cop-

*liujl@hrbeu.edu.cn
†stliu@hit.edu.cn

per could cause significant Ohmic loss. For decades, it has been known that the edge/surface waves can appear in a certain frequency range at the boundary between the magnetized plasma and a transparent material [54], such as one-way electromagnetic waveguide [40], magnetically switched transparency and opacity [55], and electrically controlled one-way photon flow [56]. On the other hand, at a certain angular frequency ω, the topologically protected surface states in the wave vector space common gap regions between the equifrequency surfaces of the magnetized plasma and the vacuum state have been studied in Ref. [57]. However, in these works, the connection between the topological invariants and edge/surface states of materials is not presented. The specific relation between edge states (frequency space common gap region) and topological invariants in magnetized plasma was first proved by Silveirinha [58], and the topological insulators in photonic crystals were extended to electromagnetic metamaterials. Recently, magnetized plasma has gained renewed interest in the context of topological edge states [22], bulk-edge correspondence [23], and Weyl semimetals [24].

In this work, we study the topological transitions and realize the nonreciprocal optical isolator in the magnetized plasma. The topological phase diagrams and the conditions for the critical points of topological transitions in magnetized plasma are shown. We demonstrate the topological transitions of the equifrequency surfaces from the closed-form ellipsoid to the open hyperboloid forms. We use the theory of Chern number of equifrequency surface [59] to study the topologically protected propagation property of surface waves at the interface between an isotropy dielectric and the magnetized plasma. Remarkably, a new type of optical isolator is demonstrated based on the leaky modes in the 3D layered structure. It is caused by breaking the time-reversal symmetry using an external magnetic field. Specifically, nonreciprocal optical isolation can occur at the interface between the isotropy dielectric layer and magnetized plasma in the 3D stratified structure.

The paper is organized as follows. In Sec. II, the topological phase diagrams and topological transitions in magnetized plasma are investigated. In Sec. III, the surface states and leaky modes in magnetized plasma are given. The leaky mode-induced optical isolators based on the 3D stratified structure are shown in Sec. IV. The conclusions are given in Sec. V.

II. TOPOLOGICAL PHASE DIAGRAMS AND TOPOLOGICAL TRANSITIONS IN MAGNETIZED PLASMA

Under the external magnetic field, electromagnetic properties of the lossless magnetized plasma along the z direction can be described as the Drude model $\epsilon_z = 1 - \omega_p^2/\omega^2$, where $\omega_p = \sqrt{Ne^2/\epsilon_0 m}$ is the plasma frequency, N represents the electron concentration, e indicates the electron charge, and m is the electron effective mass. However, the Lorentz force, induced by a nonzero magnetic field, drives the electrons to move in a plane perpendicular to the field. It eventually results in the presence of off-diagonal elements (g) in the in-plane direction. The permittivity of magnetized plasma can take the form of a tensor as [60]

$$\overline{\boldsymbol{\epsilon}}_m = \begin{pmatrix} \epsilon_t & ig & 0 \\ -ig & \epsilon_t & 0 \\ 0 & 0 & \epsilon_z \end{pmatrix}, \tag{1}$$

where $\epsilon_t = 1 - \omega_p^2/(\omega^2 - \omega_B^2)$ and $g = \omega_B\omega_p^2/[\omega(\omega^2 - \omega_B^2)]$. The ω and ω_B represent the angular frequency and the cyclotron frequency, respectively. Moreover, magnetized plasma has an isotropic permeability $\overline{\boldsymbol{\mu}}_m = \boldsymbol{I}$, where $\boldsymbol{I}$ is the identity matrix.

The constitutive relation in magnetized plasma can be described as

$$\begin{pmatrix} \mathbf{D} \\ \mathbf{B} \end{pmatrix} = \begin{pmatrix} \overline{\boldsymbol{\epsilon}}_m & 0 \\ 0 & \overline{\boldsymbol{\mu}}_m \end{pmatrix} \begin{pmatrix} \mathbf{E} \\ \mathbf{H} \end{pmatrix}. \tag{2}$$

Combining $\nabla \times \mathbf{E} = i\omega\mathbf{B}$ and $\nabla \times \mathbf{H} = -i\omega\mathbf{D}$, Maxwell's equations can be written in a 6×6 matrix form,

$$\left[\begin{pmatrix} i\overline{\boldsymbol{\kappa}} & 0 \\ 0 & i\overline{\boldsymbol{\kappa}} \end{pmatrix} - i\omega \begin{pmatrix} \boldsymbol{I} & 0 \\ 0 & -\boldsymbol{I} \end{pmatrix} \begin{pmatrix} 0 & \overline{\boldsymbol{\mu}}_m \\ \overline{\boldsymbol{\epsilon}}_m & 0 \end{pmatrix} \right] \begin{pmatrix} \mathbf{E} \\ \mathbf{H} \end{pmatrix} = 0, \tag{3}$$

where $\overline{\boldsymbol{\kappa}}$ is the skew-symmetric tensor of the wave vector $\mathbf{k}$. Then, the wave propagation of the magnetic field $\mathbf{H}$ in magnetized plasma is given by

$$[\overline{\boldsymbol{\kappa}} \cdot (\omega\overline{\boldsymbol{\epsilon}}_m)^{-1} \cdot \overline{\boldsymbol{\kappa}} + \omega\overline{\boldsymbol{\mu}}_m]\mathbf{H} = 0. \tag{4}$$

Equation (4) is the master equation of magnetized plasma, and can be written in the component form

$$\begin{pmatrix} \frac{\omega k_y^2}{\omega_p^2-\omega^2} + \frac{a}{b} & \frac{\omega k_x k_y}{-\omega_p^2+\omega^2} + \frac{i\omega_p^2\omega_B k_z^2}{b} & -\frac{[\omega(\omega_p^2+\omega_B^2-\omega^2)k_x + i\omega_p^2\omega_B k_y]k_z}{b} \\ \frac{\omega k_x k_y}{-\omega_p^2+\omega^2} - \frac{i\omega_p^2\omega_B k_z^2}{b} & \frac{\omega k_x^2}{\omega_p^2-\omega^2} + \frac{a}{b} & \frac{[i\omega_p^2\omega_B k_x + \omega(-\omega_p^2-\omega_B^2+\omega^2)k_y]k_z}{b} \\ -\frac{[\omega(\omega_p^2+\omega_B^2-\omega^2)k_x - i\omega_p^2\omega_B k_y]k_z}{b} & -\frac{[i\omega_p^2\omega_B k_x + \omega(\omega_p^2+\omega_B^2-\omega^2)k_y]k_z}{b} & \frac{d}{b} \end{pmatrix} \begin{pmatrix} H_x \\ H_y \\ H_z \end{pmatrix} = 0, \tag{5}$$

where $a = \omega[\omega_p^4 - 2\omega_p^2\omega^2 - \omega_B^2\omega^2 + \omega^4 + (\omega_p^2 + \omega_B^2 - \omega^2)k_z^2]$, $b = \omega_p^4 - 2\omega_p^2\omega^2 - \omega_B^2\omega^2 + \omega^4$, and $d = \omega[\omega_p^4 - 2\omega_p^2\omega^2 - \omega_B^2\omega^2 + \omega^4 + (\omega_p^2 + \omega_B^2 - \omega^2)(k_x^2 + k_y^2)]$, respectively.

The existence of nontrivial solutions for $\mathbf{H}$ fields requires that the determinant of the above square matrix [Eq. (5)] is zero. The condition of zero determinant gives rise to the characteristic equation of the magnetized plasma as

$$\omega^2\left(\omega_p^2 + \omega_B^2 - \omega^2\right)\left(k_x^4 + k_y^4\right) + k_y^2 e + k_x^2\left[e + 2\omega^2\left(\omega_p^2 + \omega_B^2 - \omega^2\right)k_y^2\right] + \left(\omega_p^2 - \omega^2\right)f = 0, \tag{6}$$

where $e = (\omega^2[2\omega_p^4 - 2\omega_B^2\omega^2 + 2\omega^4 + \omega_p^2(\omega_B^2 - 4\omega^2)] + [-\omega_p^2(\omega_B^2 - 2\omega^2) + 2\omega^2(\omega_B^2 - \omega^2)]k_z^2)$ and $f = [\omega^2(\omega_p^4 - 2\omega_p^2\omega^2 - \omega_B^2\omega^2 + \omega^4) + 2\omega^2(\omega_p^2 + \omega_B^2 - \omega^2)k_z^2 + (-\omega_B^2 + \omega^2)k_z^4]$.

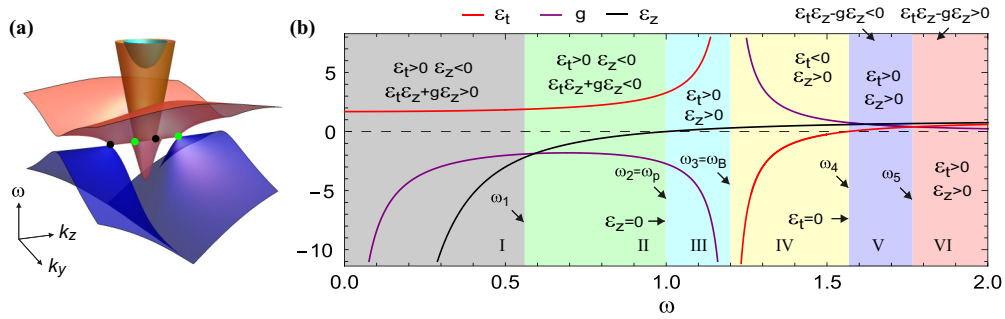

FIG. 1. Band structure and topological transition diagram in magnetized plasma. (a) Band structure and Weyl points of magnetized plasma. The green and black dots indicate the Weyl points with positive and negative chirality, respectively. (b) The change in the values of ϵ_t, g, and ϵ_z as the angular frequency ω varies. The roman numerals I–VI indicate six different phases.

Here and in the following sections, all the wave vectors are specified in units of $k_p(k_p = \omega_p/c)$, and the angular frequency ω is normalized by ω_p. Based on Eq. (6), the band structure for the magnetized plasma with $k_x = 0$ and $\omega_B > \omega_p(\omega_B = 1.2\omega_p)$ can be obtained, as shown in Fig. 1(a). Following the experimental works of Refs. [61,62], the magnetized plasma has the density (electron concentration) $N = 4.5 \times 10^{12}\text{cm}^{-3}$ [Eq. (1)], and the corresponding plasma frequency ω_p is given by $\omega_p = 1.2 \times 10^{11}\text{rad/s}$ [59]. When the cyclotron frequency $\omega_B > \omega_p(\omega_B = 1.2\omega_p)$, the strength of the applied magnetic field is 0.68T. It can be readily achieved under laboratory conditions [63]. Moreover, $\omega_B > \omega_p$ can also be realized in a certain doped semiconductor at terahertz frequency, such as InSb [62]. It behaves as the magnetized plasma for the electromagnetic waves at the terahertz band. Due to the small effective mass of electrons $m^* = 0.014m_0$, the minimum strength of the applied magnetic field $\omega_B > \omega_p$ is only 0.15T. It is completely within the range of normal experimental conditions [64].

In the band structure, there are Weyl degeneracies (green and black dots) due to the interaction of transverse mode and longitudinal mode [25]. Equation (6) is a biquadratic equation possessing higher-order dispersion, and is also known as the Fresnel equation of wave normal direction. It determines the dispersion relation, that is, the angular frequency ω as a function of the wave vector $\mathbf{k}$. At a fixed angular frequency, Eq. (6) can define the equifrequency surface of the wave vector space. Moreover, we only consider the frequency bands with $\omega > 0$ in the present study, because the mode at $(-\mathbf{k}, -\omega)$ represents the same physical mode as that at $(\mathbf{k}, \omega)$.

Along the z axis, i.e., $k_x = k_y = 0$, the characteristic equation of Eq. (6) is further given by

$$\left(\omega_p^2 - \omega^2\right)\left[\omega^2\left(\omega_p^4 - 2\omega_p^2\omega^2 - \omega_B^2\omega^2 + \omega^4\right) + 2\omega^2\left(\omega_p^2 + \omega_B^2 - \omega^2\right)k_z^2 + \left(-\omega_B^2 + \omega^2\right)k_z^4\right] = 0. \tag{7}$$

Equation (7) can then be solved to give the dispersion relation as

$$k_{z1}^{\pm} = \pm\frac{i\sqrt{\omega}\sqrt{\omega_p^2 + (\omega_B - \omega)\omega}}{\sqrt{-\omega_B + \omega}}, \quad k_{z2}^{\pm} = \pm\frac{\sqrt{\omega[-\omega_p^2 + (\omega_B + \omega)\omega]}}{\sqrt{\omega_B + \omega}}. \tag{8}$$

Then, the angular frequency threshold of the magnetized plasma [Fig. 1(b)] can be obtained as

$$\omega_1 = \frac{-\omega_B + \sqrt{4\omega_p^2 + \omega_B^2}}{2}, \quad \omega_5 = \frac{\omega_B + \sqrt{4\omega_p^2 + \omega_B^2}}{2}. \tag{9}$$

The conditions for $\epsilon_z = 0$ and $\epsilon_t = 0$ are $\omega_2 = \omega_p$ and $\omega_4 = \sqrt{\omega_p^2 + \omega_B^2}$, respectively. Moreover, a resonance frequency $\omega_3 = \omega_B(|\epsilon_t| = |g| \to \infty)$ exists in the magnetized plasma.

The dispersion features of the components of Eq. (1) are plotted in Fig. 1(b). In the figure, we distinguish the phase diagram of different electromagnetic parameter combinations by roman numerals I–VI. They are as follows: $\epsilon_t > 0$, $\epsilon_z < 0$, and $\epsilon_t\epsilon_z + g\epsilon_z > 0$ in region I; $\epsilon_t > 0$, $\epsilon_z < 0$, and $\epsilon_t\epsilon_z + g\epsilon_z < 0$ in region II; $\epsilon_t > 0$ and $\epsilon_z > 0$ in region III; $\epsilon_t < 0$ and $\epsilon_z > 0$ in region IV; $\epsilon_t > 0$, $\epsilon_z > 0$, and $\epsilon_t\epsilon_z - g\epsilon_z < 0$ in region V; $\epsilon_t > 0$, $\epsilon_z > 0$, and $\epsilon_t\epsilon_z - g\epsilon_z > 0$ in region VI.

In magnetized plasma, different topology forms of equifrequency surface arise from the relation between the dielectric tensor components [Eq. (1)]. Thus, changing the angular frequency can essentially vary the equifrequency surface. There are significant differences in the equifrequency surface topology at different angular frequencies in the magnetized plasma, as shown in Fig. 2. The equifrequency surfaces are symmetric about the $x - y$ plane. If $\omega \to 0$, the components g and ϵ_z approaches infinity. In this case, the radius of the equifrequency surface of the magnetized plasma becomes very large, so the equifrequency surfaces are two flat planes in the wave vector space, as shown in Fig. 2(a). In the phase I region, $k_{z2}^{\pm}$ [Eq. (8)] are nonphysical solutions because of $\epsilon_t\epsilon_z + g\epsilon_z > 0$. The equifrequency surface becomes a twofold type-I hyperboloid, as illustrated in Fig. 2(b). However, there is an interesting feature of equifrequency surfaces in region II,

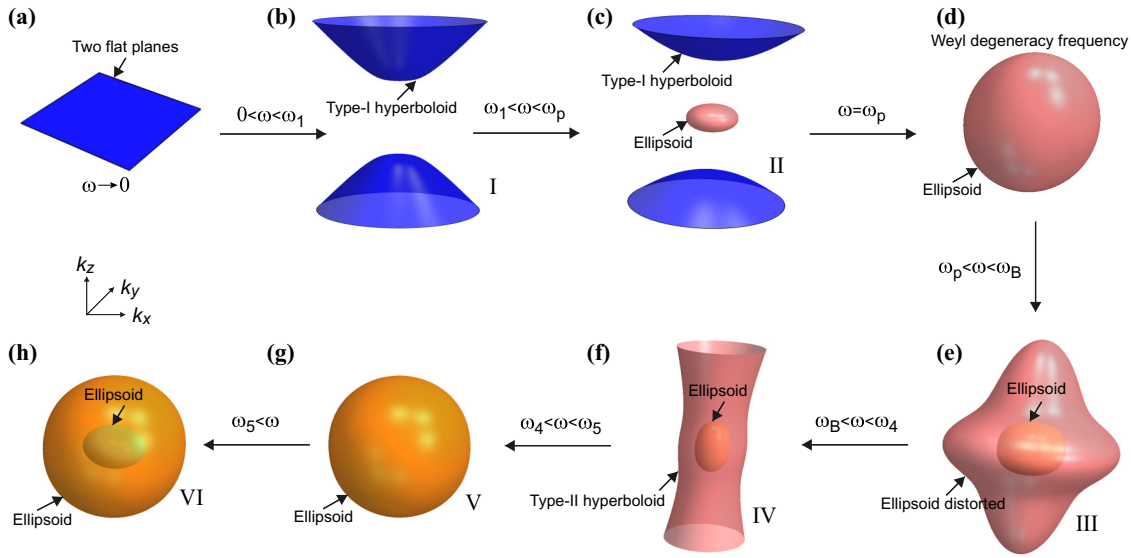

FIG. 2. Equifrequency surfaces and topological transitions. (a) Highly anisotropic medium when the angular frequency $\omega \to 0$. (d) The ellipsoidal equifrequency surface at Weyl degeneracy frequency $\omega = 1.0\omega_p$. (b), (c), (e)–(h) The equifrequency surfaces caused by the change of angular frequency ω: (b) $\omega = 0.4\omega_p$, (c) $\omega = 0.67\omega_p$, (e) $\omega = 1.1\omega_p$, (f) $\omega = 1.3\omega_p$, (g) $\omega = 1.7\omega_p$, and (h) $\omega = 1.8\omega_p$, corresponding to phase I–VI regions in Fig. 1(b), respectively.

which contains the ellipsoid and a twofold type-I hyperboloid along the z axis, as shown in Fig. 2(c). It is called the mixed-type dispersion. Once the condition $\omega = \omega_p$ is satisfied, the equifrequency surface is a single ellipsoid because there are Weyl points ($\epsilon_z = 0$) along the z-axis direction, as illustrated in Fig. 2(d). In the phase III region, the magnetized plasma exists as two separate ellipsoids and the pink equifrequency surface is stretched along the z axis, as shown in Fig. 2(e). From the phase III to phase IV regions, the pink equifrequency surface changes from a closed ellipsoid to an open type-II hyperboloid, and the middle orange ellipsoid keeps its topology unchanged, as described in Fig. 2(f). Similar to region I, there is only one ellipsoidal equifrequency surface in the phase V region. In this case, $k_{z1}^{\pm}$ [Eq. (8)] are nonphysical solutions owing to $\epsilon_t\epsilon_z - g\epsilon_z < 0$. Moreover, two ellipsoid equifrequency surfaces exist in region VI. The resulting forms of equifrequency surfaces are caused by the time-reversal symmetry breaking. Hence, the topological transitions of the equifrequency surfaces from a closed-form ellipsoid to the open forms type-I or type-II hyperboloid can be realized by only changing the angular frequency ω [Fig. 1(a)] in the magnetized plasma, as shown in Fig. 2.

III. SURFACE STATES AND LEAKY MODES

As illustrated in Figs. 3(a) and 3(e), we consider the 3D stratified structures along the x axis and translation-invariant in the y–z plane. For the isotropic medium-magnetized plasma structure in Fig. 3(a), the surface states can be obtained by matching the tangential boundary condition of Maxwell's equations [14]. The topological surface states at the interface between an isotropy dielectric $\epsilon_d = 1.1 + 0.001i$ and the magnetized plasma with $\omega = 0.67\omega_p$ and $\omega_B = 1.2\omega_p$. In Fig. 3(b), the gray regions represent the common band gap in the wave vector space. The surface states are colored with red and black lines. The blue lines and the green dotted line represent the equifrequency surfaces of the magnetized plasma and isotropy dielectric, respectively. It is worth noting that in the topological phase diagram of Fig. 1(b), the existence of stable band gaps [corresponding to the phase I and II regions in Fig. 1] of the equifrequency surfaces of the magnetized plasma is a prerequisite for the realization of the topological surface states [Fig. 3(b)] and the nonreciprocal optical isolation [Fig. 3(f)] in the wave vector space. In particular, $\omega = 0.67\omega_p$ [corresponding to the phase II region in Fig. 1(b)] is taken as a prototype to realize the nonreciprocal optical isolator in the magnetized plasma, as shown in Fig. 3. In the common band gap [gray shadow region in Fig. 3(b)] of the magnetized plasma and isotropic medium, the existence of the topological surface state is guaranteed by the different gap Chern numbers of the two materials (bulk-edge correspondence) [23,65]. Moreover, the topologically protected photonic surface states [Fig. 3(b)] are robust against disorder on all length scales and for a wide range of medium electromagnetic parameters [14]. The LEP and REP represent left and right elliptical polarizations of the topological surface states, respectively. The topological surface states connect the dielectric (green dotted circle) and the magnetized plasma (blue lines), as shown in Fig. 3(b). The Chern number of each equifrequency surface in magnetized plasma can be obtained by the generalized Gauss-Bonnet theorem [59]. Figures 3(c) and 3(d) show the topologically protected propagation property of the surface waves. They can bypass the square defect and transmit stably. The simulation results represent the field patterns E_z.

In Fig. 3(e), two different isotropic media with permittivities ϵ_d and ϵ_p occupy the regions $0 < x < d$ (isotropic medium) and $x > d$ (prism), respectively. The magnetized plasma with permittivity tensor $\bar{\boldsymbol{\epsilon}}_m$ fills the region $x < 0$. We use the method proposed by Dyakonov [66] to calculate the leaky modes in the 3D stratified structure [Fig. 3(e)]. According to Maxwell's equations, the eigenfields on each media in

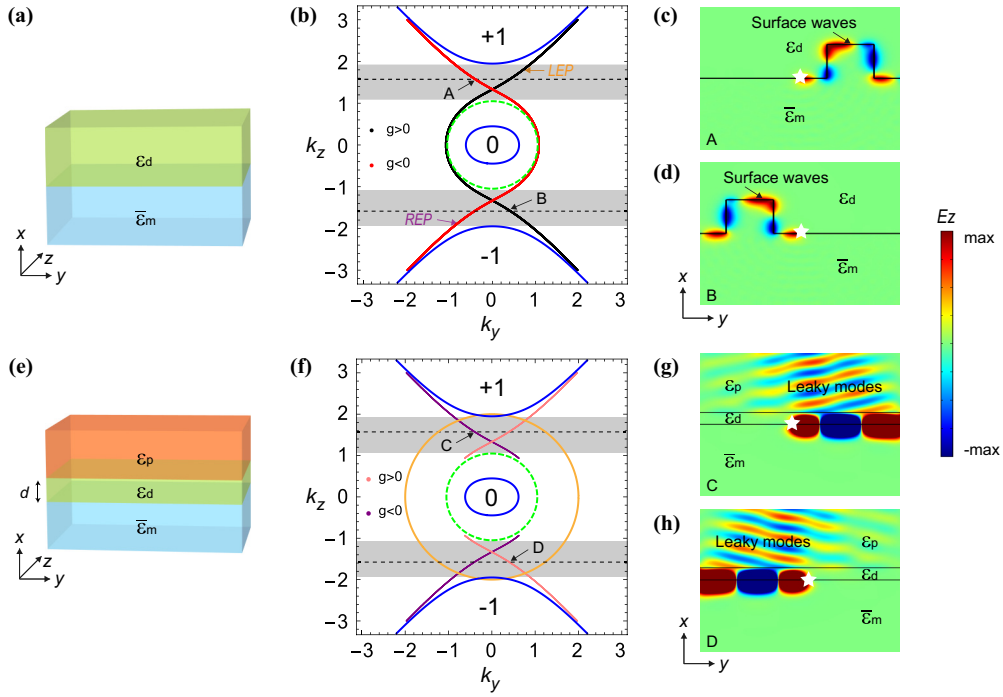

FIG. 3. Surface states and leaky modes. (a) The interface between an isotropy dielectric layer (top) and the magnetized plasma (bottom). (b) Surface states between the magnetized plasma and isotropy dielectric. (c, d) Simulation of the topological surface waves with $k_z = 1.58$ in COMSOL frequency domain, corresponding to points A and B in (b), respectively. (e) The geometry of the three-layered system. (f) The leaky modes in the 3D stratified structure. (g, h) The electric field E_z distributions for the leaky modes, corresponding to points ($k_z = 1.58$) C and D in (f), respectively. The white pentagrams represent the exciting source.

Fig. 3(e) are given by the nontrivial solutions of **E** and **H**. In the prism ϵ_p region, the two eigenmodes can be described as

$$\begin{aligned}\mathbf{E}_1 &= (-k_y k_{xp}, i(k_y^2 - \epsilon_p), ik_y k_z),\\ \mathbf{H}_1 &= (i\epsilon_p k_z, 0, \epsilon_p k_{xp}),\end{aligned} \tag{10}$$

$$\begin{aligned}\mathbf{E}_2 &= (k_z k_{xp}, -ik_y k_z, -i(k_z^2 - \epsilon_p)),\\ \mathbf{H}_2 &= (i\epsilon_p k_y, \epsilon_p k_{xp}, 0),\end{aligned} \tag{11}$$

where $k_{xp} = \sqrt{-\epsilon_p + k_y^2 + k_z^2}$ is the normal direction wave vector in the prism region.

In the isotropic medium ϵ_d, the two eigenmodes are

$$\begin{aligned}\mathbf{E}_3 &= \left[-k_y k_{xd}, i\left(k_y^2 - \epsilon_d\right), ik_y k_z\right],\\ \mathbf{H}_3 &= (ik_z\epsilon_d, 0, k_{xd}\epsilon_d),\end{aligned} \tag{12}$$

$$\begin{aligned}\mathbf{E}_4 &= \left[k_z k_{xd}, -ik_y k_z, -i\left(k_z^2 - \epsilon_d\right)\right],\\ \mathbf{H}_4 &= (ik_y\epsilon_d, k_{xd}\epsilon_d, 0),\end{aligned} \tag{13}$$

where $k_{xd} = \sqrt{k_y^2 + k_z^2 - \epsilon_d}$ is the normal direction wave vector.

Similarly, two eigenstates in the magnetized plasmas can be expressed as

$$\mathbf{E}_5 = (E_{5x}, E_{5y}, E_{5z}), \mathbf{H}_5 = (H_{5x}, H_{5y}, H_{5z}), \tag{14}$$

$$\mathbf{E}_6 = (E_{6x}, E_{6y}, E_{6z}), \mathbf{H}_6 = (H_{6x}, H_{6y}, H_{6z}). \tag{15}$$

Then, applying electromagnetic boundary conditions at $x = 0$ and $x = d$ for the tangential electric and magnetic fields leads to the determinant problem of a 8×8 constraint matrix **M**,

$$\mathrm{Det}[\mathbf{M}] = \begin{vmatrix} e^{k_{xp}d}E_{1y} & e^{k_{xp}d}E_{2y} & e^{k_{xd}d}E_{3y} & e^{k_{xd}d}E_{4y} & 0 & 0 & 0 & 0\\ e^{k_{xp}d}E_{1z} & e^{k_{xp}d}E_{2z} & e^{k_{xd}d}E_{3z} & e^{k_{xd}d}E_{4z} & 0 & 0 & 0 & 0\\ e^{k_{xp}d}H_{1y} & e^{k_{xp}d}H_{2y} & e^{k_{xd}d}H_{3y} & e^{k_{xd}d}H_{4y} & 0 & 0 & 0 & 0\\ e^{k_{xp}d}H_{1z} & e^{k_{xp}d}H_{2z} & e^{k_{xd}d}H_{3z} & e^{k_{xd}d}H_{4z} & 0 & 0 & 0 & 0\\ 0 & 0 & 0 & 0 & E_{3y} & E_{4y} & E_{5y} & E_{6y}\\ 0 & 0 & 0 & 0 & E_{3z} & E_{4z} & E_{5z} & E_{6z}\\ 0 & 0 & 0 & 0 & H_{3y} & H_{4y} & H_{5y} & H_{6y}\\ 0 & 0 & 0 & 0 & H_{3z} & H_{4z} & H_{5z} & H_{6z} \end{vmatrix} = 0. \tag{16}$$

The leaky modes of the three-layer structure are as follows: the semi-infinite prism layer (orange) and the magnetized plasma (light blue) are separated by a thin isotropy dielectric layer (light green), as depicted in Fig. 3(e). The magne-

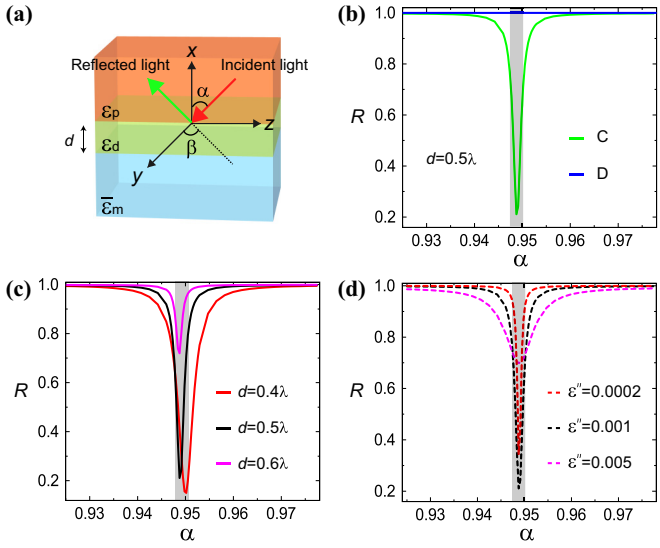

FIG. 4. Leaky mode-induced optical isolators based on the 3D stratified structure. (a) Schematic of the obliquely incident electromagnetic wave of the 3D layered structure composed of a prism layer (orange), an isotropy dielectric layer (light green), and the magnetized plasma (light blue). The layers are infinite in the y–z plane. (b) The nonreciprocal optical isolation with $d = 0.5\lambda$ and $\epsilon'' = 0.001$, corresponding to points C and D in Fig. 3(f), respectively. (c) The reflectivity of the nonreciprocal optical isolation for different thickness values of the isotropy dielectric. (d) The reflectivity of the nonreciprocal optical isolation for different imaginary part values of the isotropy dielectric. The angular frequency $\omega = 0.67\omega_p$ and cyclotron frequency $\omega_B = 1.2\omega_p$ for all the plots.

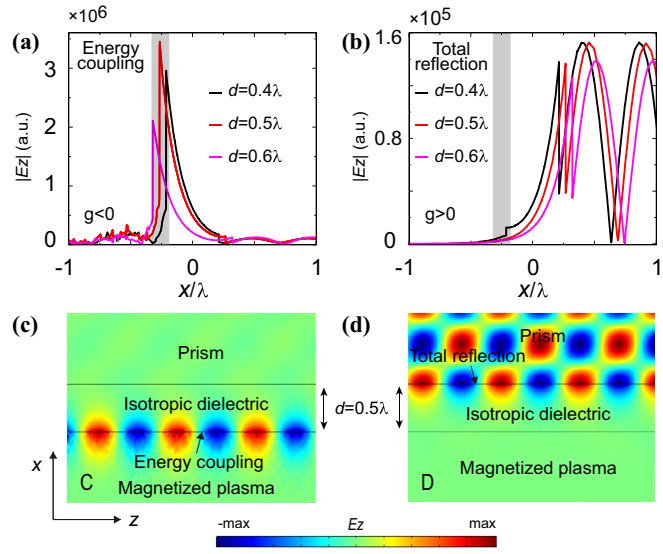

FIG. 5. Nonreciprocal energy coupling. (a, b) Profiles of the electric field (E_z) along the direction of the 3D layered structure with different thickness values d. The imaginary part value of the isotropy dielectric is $\epsilon'' = 0.001$. (c, d) Field of points C and D [Fig. 3(f)] distribution simulated by COMSOL MULTIPHYSICS. The electromagnetic parameters of the magnetized plasma are in accordance with Fig. 4.

tized plasma is covered with an isotropy dielectric cover of the thickness $d = 0.5\lambda(\lambda = 2\pi c/\omega)$. In Fig. 3(f), the leaky modes can be obtained based on Eq. (16). The blue lines, orange line, and green dotted line represent the equifrequency surfaces of the magnetized plasma, prism, and isotropy dielectric, respectively. Notably, the modes (pink and purple lines) located in the shadow part are not a surface state because they are surrounded by the prism bulk state, as shown in Fig. 3(f). Thus, they will leak energy to the prism side, forming the leaky modes, as illustrated in Figs. 3(g) and 3(h). The leaky modes are excited by an electric-line source at the interface between the isotropy dielectric and magnetized plasma. Moreover, the permittivities of the isotropy medium and prism layer in Figs. 3(e)–3(h) are $\epsilon_d = 1.1 + 0.001i$ and $\epsilon_p = 4$, respectively.

IV. REALIZATION OF THE LEAKY MODE-INDUCED OPTICAL ISOLATORS BASED ON THE 3D STRATIFIED STRUCTURE

For the 3D structure in Fig. 4(a), the obliquely incident wave has the azimuthal angle α and project angle β. Here, $\beta = \arctan(k_y/k_z)$ is located in the y–z plane. The permittivities of the prism and isotropy dielectric layer are $\epsilon_p = 4$ and $\epsilon_d = 1.1 + i\epsilon''$, respectively. The small imaginary value ϵ'' is used to achieve the nonreciprocal optical isolation, i.e., the incident wave energy can be coupled to the surface modes between the isotropic dielectric and a magnetized plasma [Fig. 3(b)]. The time-reversal symmetry is broken for the leaky modes because of the nonzero external magnetic field, as illustrated in Fig. 3(f). Specifically, for point C, the optical isolation can be realized when the azimuth angle α changes. However, for point D, the incident light always occurs as total reflection ($R = 1.0$), as shown in Fig. 4(b). The reflectivity (R) in the optical isolator [Fig. 4(a)] can be calculated by COMSOL MULTIPHYSICS.

The reflectivity (R) correspondingly changes for different thicknesses d and imaginary parts ϵ'' of the isotropy dielectric [Fig. 4(a)]. Notably, for different thicknesses d of the medium layer, the angle of nonreciprocal optical isolation will also change, as shown by Fig. 4(c). On the other hand, for different small imaginary values ϵ'' of the dielectric layer [Fig. 4(a)], the angle of nonreciprocal optical isolation does not change, as illustrated in Fig. 4(d). However, the nonreciprocal optical isolation at a specific azimuthal angle α of the obliquely incident wave can be achieved in both cases of Figs. 4(c) and 4(d).

We further verify the nonreciprocal coupling ($g < 0$) from the view of the electric field distribution with different thicknesses d of the isotropic medium layer, as shown in Fig. 5(a). In these cases, the field energy is mainly concentrated at the interface between the isotropic dielectric and the magnetized plasma. On the other hand, no energy coupling occurs when the direction of the magnetic field is reversed ($g > 0$), as shown in Fig. 5(b). The incident light is all reflected only at the interface between the isotropic dielectric and the prism. Figures 5(c) and 5(d) show the field E_z distribution of the nonreciprocal optical isolation, corresponding to points C and D in Fig. 3(f), respectively. Therefore, a new type of optical isolator can be realized in the 3D stratified structure, as shown in Figs. 5(c) and 5(d).

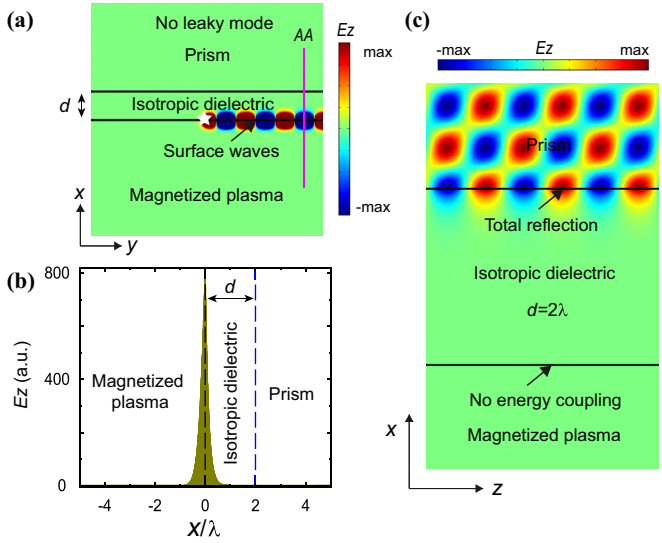

FIG. 6. One-way surface modes. (a) The electric field distributions for the one-way surface modes, corresponding to point A in Fig. 3(b). The imaginary part value of the isotropy dielectric is $\epsilon'' = 0.001$. (b) One-dimensional electric field profiles E_z at line AA in (a). (c) Distribution of electric field E_z.

The skin depth of surface wave in the medium can be determined by the penetration distance of the electric field down to $1/e$. The skin depth in the isotropic dielectric is described as $d_s/\lambda = 1/\mathrm{Im}(k_{xd})$ because the imaginary part of the wave vector k_{xd} at the boundary causes exponential attenuation of the electric field. The skin depth of the isotropic dielectric at point A [Fig. 3(b)] is $d_s/\lambda = 1/\mathrm{Im}(\sqrt{1 - 1.58^2 - |-0.4|^2}) \approx 0.78$. In Fig. 6(a), the magnetized plasma is covered with an isotropy dielectric cover of thickness $d = 2\lambda > 2d_s$. In this case, the isotropy dielectric coating completely prevents the coupling from the lower to the upper boundary. Therefore, the one-way surface mode only exists at the isotropy dielectric-magnetized plasma interface and does not radiate into prism half-space, as shown in Fig. 6(a). One-dimensional electric field profile E_z at line AA in Fig. 6(a) is shown, as illustrated in Fig. 6(b). Indeed, the surface wave is only localized at the interface between the isotropy dielectric and magnetized plasma. It directly verifies that the surface mode [Fig. 6(a)] cannot be coupled to the prism region. Thus, similar to Fig. 5(d), the incident light is all reflected at the interface between the isotropic dielectric and prism layer, as shown in Fig. 6(c).

V. CONCLUSIONS

In conclusion, the topology of equifrequency surfaces in the magnetized plasma is investigated. The topological phase diagrams and the critical points of topological transitions are given. Based on different types of equifrequency surfaces, the topological transitions are confirmed in magnetized plasma. The topologically protected propagation property of surface waves at the interface between the magnetized plasma and an isotropy dielectric medium is revealed. The leaky modes can be obtained by a three-layered media system. The semi-infinite prism layer and magnetized plasma are separated by a thin isotropy dielectric layer. Notably, we demonstrate a design of optical isolators based on the 3D layered structure. The isolation property of the optical isolators is related to the azimuthal angle and projection angle of the obliquely incident light. Moreover, the direction of the nonreciprocal coupling can be reconfigurable by simply adjusting the external magnetic field of the 3D stratified structure. This work may have potential applications for new high-performance nonreciprocal optical devices.

ACKNOWLEDGMENTS

This work was supported by the National Natural Science Foundation of China (NSFC) (Grants No. 61575055, No. 11874132, No. 12074087, and No. 11974428).

The authors declare no conflicts of interest.

[1] M. Z. Hasan and C. L. Kane, *Colloquium:* Topological insulators, Rev. Mod. Phys. **82**, 3045 (2010).

[2] L. Lu, J. D. Joannopoulos, and M. Soljačić, Topological photonics, Nat. Photonics **8**, 821 (2014).

[3] A. B. Khanikaev and G. Shvets, Two-dimensional topological photonics, Nat. Photonics **11**, 763 (2017).

[4] S. Weidemann, M. Kremer, T. Helbig, T. Hofmann, A. Stegmaier, M. Greiter, R. Thomale, and A. Szameit, Topological funneling of light, Science, **368**, 311 (2020).

[5] T. Ozawa, H. M. Price, A. Amo, N. Goldman, M. Hafezi, L. Lu, M. C. Rechtsman, D. Schuster, J. Simon, O. Zilberberg, and I. Carusotto, Topological photonics, Rev. Mod. Phys. **91**, 015006 (2019).

[6] Y. Z. Liu, X. B. Chen, and Y. Xu, Topological phononics: From fundamental models to real materials, Adv. Funct. Mater. **30**, 1904784 (2020).

[7] S. A. R. Horsley and M. Woolley, Zero-refractive-index materials and topological photonics, Nat. Phys. **17**, 348 (2021).

[8] A. B. Khanikaev, S. H. Mousavi, W. K. Tse, M. Kargarian, A. H. MacDonald, and G. Shvets, Photonic topological insulators, Nat. Mater. **12**, 233 (2013).

[9] C. He, X. C. Sun, X. P. Liu, M. H. Lu, Y. Chen, L. Feng, and Y. F. Chen, Photonic topological insulator with broken time-reversal symmetry, Proc. Natl. Acad. Sci. USA **113**, 4924 (2016).

[10] X. Cheng, C. Jouvaud, X. Ni, S. H. Mousavi, A. Z. Genack, and A. B. Khanikaev, Robust reconfigurable electromagnetic pathways within a photonic topological insulator, Nat. Mater. **15**, 542 (2016).

[11] Y. Yang, Z. Gao, H. Xue, L. Zhang, M. He, Z. Yang, R. Singh, Y. D. Chong, B. L. Zhang, and H. Chen, Realization of a three-

dimensional photonic topological insulator, Nature (London) **565**, 622 (2019).
[12] W. Zhu, H. Xue, J. Gong, Y. Chong, and B. Zhang, Time-periodic corner states from Floquet higher-order topology, Nat. Commun. **13**, 11 (2022).
[13] R. Gladstein Gladstone, M. Jung, and G. Shvets, Spin-Polarized Fractional Corner Charges and Their Photonic Realization, Phys. Rev. Lett. **128**, 026801 (2022).
[14] W. Gao, M. Lawrence, B. Yang, F. Liu, F. Fang, B. Béri, J. Li, and S. Zhang, Topological Photonic Phase in Chiral Hyperbolic Metamaterials, Phys. Rev. Lett. **114**, 037402 (2015).
[15] J. Hou, Z. Li, X. Luo, Q. Gu, and C. Zhang, Topological Bands and Triply Degenerate Points in Non-Hermitian Hyperbolic Metamaterials, Phys. Rev. Lett. **124**, 073603 (2020).
[16] J. Hou, Z. Li, Q. Gu, and C. Zhang, Topological and hyperbolic dielectric materials from chirality-induced charge-parity symmetry, Phys. Rev. A **104**, 043510 (2021).
[17] Z. Wang, Y. Chong, J. D. Joannopoulos, and M. Soljačić, Observation of unidirectional backscattering-immune topological electromagnetic states, Nature (London) **461**, 772 (2009).
[18] S. A. Skirlo, L. Lu, and M. Soljačić, Multimode One-Way Waveguides of Large Chern Numbers, Phys. Rev. Lett. **113**, 113904 (2014).
[19] S. A. Skirlo, L. Lu, Y. Igarashi, Q. Yan, J. D. Joannopoulos, and M. Soljačić, Experimental Observation of Large Chern Numbers in Photonic Crystals, Phys. Rev. Lett. **115**, 253901 (2015).
[20] J. You, Q. Ma, Z. Lan, Q. Xiao, N. C. Panoiu, and T. Cui, Reprogrammable plasmonic topological insulators with ultrafast control, Nat. Commun. **12**, 5468 (2021).
[21] X. Xi, X. Li, K. Ye, H. Wu, J. Chen, and R. Wu, Dual-polarization topological phases and phase transition in magnetic photonic crystalline insulator, New J. Phys. **23**, 083042 (2021).
[22] J. B. Parker, J. B. Marston, S. M. Tobias, and Z. Zhu, Topological Gaseous Plasmon Polariton in Realistic Plasma, Phys. Rev. Lett. **124**, 195001 (2020).
[23] S. A. Hassani Gangaraj and F. Monticone, Physical Violations of the Bulk-Edge Correspondence in Topological Electromagnetics, Phys. Rev. Lett. **124**, 153901 (2020).
[24] Y. Fu and H. Qin, Topological phases and bulk-edge correspondence of magnetized cold plasmas, Nat. Commun. **12**, 3924 (2021).
[25] Y. Liu, P. Wang, and S. Zhang, A nonlocal effective medium description of topological Weyl metamaterials, Laser Photonics Rev. **15**, 2100129 (2021).
[26] Q. Guo, W. Gao, J. Chen, Y. Liu, and S. Zhang, Line Degeneracy and Strong Spin-Orbit Coupling of Light with Bulk Bianisotropic Metamaterials, Phys. Rev. Lett. **115**, 067402 (2015).
[27] H. N. Krishnamoorthy, Z. Jacob, E. Narimanov, I. Kretzschmar, and V. M. Menon, Topological transitions in metamaterials, Science, **336**, 205 (2012).
[28] P. H. Chang, C. Y. Kuo, and R. L. Chern, Wave propagation in bianisotropic metamaterials: Angular selective transmission, Opt. Express **22**, 25710 (2014).
[29] P. Huo, Y. Liang, S. Zhang, Y. Lu, and T. Xu, Angular optical transparency induced by photonic topological transitions in metamaterials, Laser Photonics Rev. **12**, 1700309 (2018).
[30] Y. Gelkop, F. D. Mei, S. Frishman, Y. Garcia, L. Falsi, G. Perepelitsa, C. Conti, E. DelRe, and A. J. Agranat, Hyperbolic optics and superlensing in room-temperature KTN from self-induced k-space topological transitions, Nat. Commun. **12**, 7241 (2021).
[31] P. N. Dyachenko, S. Molesky, A. Y. Petrov, M. Stormer, T. Krekeler, S. Lang, M. Ritter, Z. Jacob, and M. Eich, Controlling thermal emission with refractory epsilon-near-zero metamaterials via topological transitions, Nat. Commun. **7**, 11809 (2016).
[32] V. R. Tuz, I. V. Fedorin, and V. I. Fesenko, Bi-hyperbolic isofrequency surface in a magnetic-semiconductor superlattice, Opt. Lett. **42**, 4561 (2017).
[33] V. I. Fesenko and V. R. Tuz, Lossless and loss-induced topological transitions of isofrequency surface in a biaxial gyroeletromagnetic medium, Phys. Rev. B **99**, 094404 (2019).
[34] R. Chern and Y. Yu, Chiral surface waves on hyperbolic-gyromagnetic metamaterials, Opt. Express **25**, 11801 (2017).
[35] Q. Guo, B. Yang, L. Xia, W. Gao, H. Liu, J. Chen, Y. Xiang, and S. Zhang, Three Dimensional Photonic Dirac Points in Metamaterials, Phys. Rev. Lett. **119**, 213901 (2017).
[36] Q. Guo, O. You, B. Yang, J. Sellman, E. Blythe, H. Liu, Y. Xiang, D. Fan, J. Chen, C. T. Chan, and S. Zhang, Observation of Three-Dimensional Photonic Dirac Points and Spin-Polarized Surface Arcs, Phys. Rev. Lett. **122**, 203903 (2019).
[37] N. Han, J. L. Liu, Y. Gao, K. Y. Zhou, and S. T. Liu, Topologically protected and highly localized surface waves in gyro-electromagnetic metamaterials, Ann. Phys. **532**, 2000022 (2020).
[38] R. C. Shiu, H. C. Chan, H. X. Wang, and G. Y. Guo, Photonic Chern insulators made of gyromagnetic hyperbolic metamaterials, Phys. Rev. Mater. **4**, 065202 (2020).
[39] D. Jalas, A. Petrov, M. Eich, W. Freude, S. Fan, Z. Yu, R. Baets, M. Popović, A. Melloni, J. D. Joannopoulos, M. Vanwolleghem, C. R. Doerr, and H. Renner, What is – and what is not – an optical isolator, Nat. Photonics **7**, 579 (2013).
[40] Z. Yu, G. Veronis, Z. Wang, and S. Fan, One-Way Electromagnetic Waveguide Formed at the Interface between a Plasmonic Metal under a Static Magnetic Field and a Photonic Crystal, Phys. Rev. Lett. **100**, 023902 (2008).
[41] D. Karki, R. E. Ganainy, and M. Levy, Toward High-Performing Topological Edge-State Optical Isolators, Phys. Rev. Appl. **11**, 034045 (2019).
[42] S. Lin, S. Silva, J. Zhou, and D. Talbayev, A one-way mirror: High-performance terahertz optical isolator based on magneto-plasmonics, Adv. Opt. Mater. **6**, 1800572 (2018).
[43] V. S. Asadchy, C. Guo, B. Zhao, and S. Fan, Sub-wavelength passive optical isolators using photonic structures based on Weyl semimetals, Adv. Opt. Mater. **8**, 2000100 (2020).
[44] J. Ma, J. Wen, S. Ding, S. Li, Y. Hu, X. Jiang, L. Jiang, and M. Xiao, Chip-based optical isolator and nonreciprocal parity-time symmetry induced by stimulated Brillouin scattering, Laser Photonics Rev. **14**, 1900278 (2020).
[45] C. Liang, B. Liu, A. Xu, X. Wen, C. Lu, K. Xia, M. K. Tey, Y. Liu, and L. You, Collision-Induced Broadband Optical Nonreciprocity, Phys. Rev. Lett. **125**, 123901 (2020).
[46] E. Z. Li, D. S. Ding, Y. C. Yu, M. X. Dong, L. Zeng, W. H. Zhang, Y. H. Ye, H. Z. Wu, Z. H. Zhu, W. Gao, G. C. Guo, and B. S. Shi, Experimental demonstration of cavity-free optical

isolators and optical circulators, Phys. Rev. Res. **2**, 033517 (2020).

[47] Y. Hu, S. Zhang, Y. Qi, G. Lin, Y. Niu, and S. Gong, Multi-wavelength Magnetic-Free Optical Isolator by Optical Pumping in Warm Atoms, Phys. Rev. Appl. **12**, 054004 (2019).

[48] S. Lannebere, D. E. Fernandes, T. A. Morgado, and M. G. Silveirinha, Nonreciprocal and Non-Hermitian Material Response Inspired by Semiconductor Transistors, Phys. Rev. Lett. **128**, 013902 (2022).

[49] Y. Ji, F. Fan, Z. Tan, and S. Chang, Terahertz nonreciprocal isolator based on magneto-plasmon and destructive interference at room temperature, Front. Phys. **8**, 334 (2020).

[50] X. Zhou, Y. Wang, D. Leykam, and Y. D. Chong, Optical isolation with nonlinear topological photonics, New J. Phys. **19**, 095002 (2017).

[51] W. C. Wong, W. Wang, W. T. Yau, and K. H. Fung, Topological theory for perfect metasurface isolators, Phys. Rev. B **101**, 121405 (2020).

[52] W. Wang, W. T. Yau, Y. Cui, J. Wang, and K. H. Fung, Maxwell's demon-like nonreciprocity by non-Hermitian gyrotropic metasurfaces, Phys. Rev. Res. **3**, L022006 (2021).

[53] B. Zhu, G. Ren, Y. Gao, B. Wu, Q. Wang, C. Wan, and S. Jian, Graphene plasmons isolator based on non-reciprocal coupling, Opt. Express **23**, 16071 (2015).

[54] J. J. Brion, R. F. Wallis, A. Hartstein, and E. Burstein, Theory of Surface Magnetoplasmons in Semiconductors, Phys. Rev. Lett. **28**, 1455 (1972).

[55] A. R. Davoyan and N. Engheta, Theory of Wave Propagation in Magnetized Near-Zero-Epsilon Metamaterials: Evidence for One-Way Photonic States and Magnetically Switched Transparency and Opacity, Phys. Rev. Lett. **111**, 257401 (2013).

[56] A. Davoyan and N. Engheta, Electrically controlled one-way photon flow in plasmonic nanostructures, Nat. Commun. **5**, 5250 (2014).

[57] B. Yang, M. Lawrence, W. Gao, Q. Guo, and S. Zhang, One-way helical electromagnetic wave propagation supported by magnetized plasma, Sci. Rep. **6**, 21461 (2016).

[58] M. G. Silveirinha, Chern invariants for continuous media, Phys. Rev. B **92**, 125153 (2015).

[59] W. Gao, B. Yang, M. Lawrence, F. Fang, B. Béri, and S. Zhang, Photonic Weyl degeneracies in magnetized plasma, Nat. Commun. **7**, 12435 (2016).

[60] S. Zhang, Y. Xiong, G. Bartal, X. Yin, and X. Zhang, Magnetized Plasma for Reconfigurable Subdiffraction Imaging, Phys. Rev. Lett. **106**, 243901 (2011).

[61] Y. P. Bliokh, J. Felsteiner, and Y. Z. Slutsker, Total Absorption of an Electromagnetic Wave by an Overdense Plasma, Phys. Rev. Lett. **95**, 165003 (2005).

[62] D. Wang, B. Yang, W. Gao, H. Jia, Q. Yang, X. Chen, M. Wei, C. Liu, M. Navarro-Cía, J. Han, W. Zhang, and S. Zhang, Photonic Weyl points due to broken time-reversal symmetry in magnetized semiconductor, Nat. Phys. **15**, 1150 (2019).

[63] Z. Abelson, R. Gad, S. Bar-Ad, and A. Fisher, Anomalous Diffraction in Cold Magnetized Plasma, Phys. Rev. Lett. **115**, 143901 (2015).

[64] X. Wang, A. A. Belyanin, S. A. Crooker, D. M. Mittleman, and J. Kono, Interference-induced terahertz transparency in a semiconductor magnetoplasma, Nat. Phys. **6**, 126 (2010).

[65] F. Monticone, A truly one-way lane for surface plasmon, Nat. Photonics **14**, 461 (2020).

[66] M. I. Dyakonov, New type of electromagnetic wave propagating at the interface, Sov. Phys. JETP **67**, 714 (1988).